# Effects of polarization on stimulated Brillouin scattering in a birefringent optical fiber

**Daisy Williams,* Xiaoyi Bao, and Liang Chen**

*Department of Physics, University of Ottawa, MacDonald Hall, 150 Louis Pasteur, Ottawa, Ontario K1N 6N5, Canada*
**Corresponding author: dwill087@uOttawa.ca*

Received May 16, 2014; revised July 19, 2014; accepted July 28, 2014;
posted July 31, 2014 (Doc. ID 211919); published September 19, 2014

The most general model of elliptical birefringence in an optical fiber has been developed for a steady-state and transient stimulated Brillouin scattering interaction. The impact of the elliptical birefringence is to induce a Brillouin frequency shift and distort the Brillouin spectrum—which varies with different light polarizations and pulsewidths. The model investigates the effects of birefringence and the corresponding evolution of spectral distortion effects along the fiber, providing a valuable prediction tool for distributed sensing applications. 

*OCIS codes:* (060.2310) Fiber optics; (190.4370) Nonlinear optics, fibers; (260.1440) Birefringence; (260.5430) Polarization; (290.5900) Scattering, stimulated Brillouin.
http://dx.doi.org/10.1364/PRJ.2.000126

## 1. INTRODUCTION

Birefringence is the optical property of a material having a refractive index that depends on the polarization and propagation direction of light [1,2]. In optical fibers, the birefringence effect is detrimental for a variety of reasons. The Brillouin gain depends on the state of polarization (SOP) in the fiber [3–6], and unintended birefringence causes the polarization of the optical field to change during propagation through the fiber, which induces power fluctuations [5], especially in the stimulated Brillouin scattering (SBS) process [4]. The local refractive index changes associated with density fluctuations cause the Brillouin spectrum shape to change and the Brillouin frequency peak position to shift [6]. Such induced Brillouin peak shift and spectral distortions may be attributed to local temperature or strain change, and cause error in distributed temperature and strain measurement [7–9]. In [10], the Brillouin gain spectra were shown to be strongly influenced by thermal stress.

It is important to devise a comprehensive characterization of the SBS process in the presence of birefringence in an optical fiber, so that a prediction of the Brillouin frequency shift and birefringence variation over different sensing lengths can be made. All previous theoretical works [3–5,11–14] are related to the Brillouin gain variation due to the SOP change. Although the effects of fiber birefringence on Brillouin frequency shift and linewidth have been studied experimentally [15], no report has been made regarding the Brillouin frequency shift associated with the SOP and birefringence change in relation to the fiber position.

A quantitative study of the fiber birefringence versus frequency shift is essential in finding the maximum impact of fiber birefringence on the measurement precision of temperature and strain, for distributed Brillouin optical time domain analysis (BOTDA) or Brillouin optical time domain reflectometry (BOTDR) sensors, as it will be helpful in designing the best suitable fiber for BOTDA or BOTDR applications as well as optimizing system design.

Among early works that investigate the polarization effects on SBS in optical fibers, Refs. [3,5,11,12] showed that the Stokes gain is strongly dependent on polarization effects, and in [16] this theoretical work was experimentally confirmed. Reference [13] examines the applications of optical birefringence in SBS sensing for strain and temperature measurements, while [4] devises a technique to overcome the sensitivity of pulse delay to polarization perturbations, enhancing SBS slow light delay. In [14], a vector formalism was used to characterize the effects of birefringence on the SBS interaction. One such effect was signal broadening as a result of polarization effects. However, only linearly polarized (LP) pump and signal waves were investigated in [13,14]. Additionally, [14] assumed an undepleted pump regime, which has applications only for short fiber lengths, while the BOTDA and BOTDR often operate on long fiber distances; the convolution of the birefringence and depletion would induce much larger distortion on the Brillouin spectrum, and hence lower the temperature and strain resolution. Thus the undepleted and LP models are not adequate to address real problems.

The above-mentioned works [5,11,12,14,16], however, treat a steady-state SBS system in which both the pump wave (PW) and the Stokes wave (SW) are continuous. Additionally, none of these references investigated the effect of birefringence and polarization effects on the spectral distortion—namely Brillouin frequency shift—of pulses undergoing SBS. In [4], though pulse length was taken into account, Brillouin spectrum distortion was not. More importantly, the impact of the nonlinear effect under different pump powers convoluted with fiber birefringence and its impact on the Brillouin spectrum shape and peak shift have not been examined yet. An extension of [14] was published in the work [17], whereby signal pulses were taken into consideration and pulse distortion was observed. However, this work still did not take into

 

consideration the most general case of birefringence, which is elliptical birefringence.

It is important to investigate a more accurate model of the polarization-dependent SBS interaction, which includes the case of elliptical birefringence. The model presented in this manuscript describes equations that can be thought of as the most comprehensive SBS equations considering the birefringence effects in an optical fiber. Besides being able to accommodate the most general case of elliptical birefringence, the effects of polarization mode dispersion (PMD), polarization dispersion loss (PDL), phonon resonance structures, pulse length, and the overall attenuation of the fiber have been taken into account.

This manuscript will introduce several important applications of birefringence in optical fibers, relating to telecommunications and fiber sensing. The effect of the spectral shift due to increased birefringence is investigated. Additionally, spectral distortion due to various degrees of birefringence will be investigated for steady-state and transient pulsed regimes. Namely, the steady-state model presented for LP light will be shown to be a valuable measure of the experimentally realistic case of nonideal LP light in optical fibers. The degree of spectral distortion may be used as an indication of the quality of linear polarization during the SBS interaction or as a measure of power leaking between the fast and slow modes. Furthermore, increased power leaking between the fast and slow modes for LP can be used to create a regime that is more favorable for sensing applications related to SBS. In the pulsed regime, spectral broadening and depletion of the Stokes spectrum will be observed as a result of increased birefringence. Spectral distortion is detrimental for fiber sensing and telecommunications; hence methods of minimizing this effect are important for these applications.

Additionally, the effects of various elliptical polarizations on output spectral shape will be investigated for the steady-state model, including spectral hole burning effects and spectral broadening. Methods for maintaining a pulse fidelity and full width at half-maximum (FWHM), as compared to nonpolarized light in a nonbirefringent fiber, will be proposed.

## 2. MODEL

The process of SBS has been studied in a birefringent polarization-maintaining optical fiber (PMF) with a core radius of 4.1 μm. The configuration is composed of a PW launched into one end, and a SW launched into the other end. Both the PW and SW have $x$ and $y$ eigenpolarization components. The schematic arrangement is shown in Fig. 1.

In the slowly varying amplitude approximation, the interaction between the PW, the SW, and the corresponding acoustic wave (AW), as shown in Fig. 1, is described by the system of Eqs. (1.1)–(1.4). Other than the usual slowly varying amplitude approximation, the only additional approximation in establishing the following equations is the assumption that the phonon fields are established almost simultaneously—which is not a bad approximation for the majority of practical cases [1,18,19]. The derivation of the system of Eqs. (1.1)–(1.4) is shown in Appendix A:

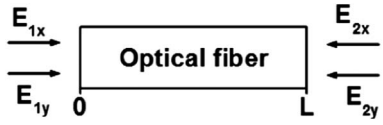


Fig. 1. Schematic arrangement of SBS in an optical fiber of length L: $E_{1x}$, PW; $E_{1y}$, PW; $E_{2x}$, SW; $E_{2y}$, SW.

$$\frac{\partial E_{1x}}{\partial z}+\frac{\bar{n}_1}{c}\frac{\partial E_{1x}}{\partial t}+\left(\bar{\alpha}_1+\frac{\Delta\bar{\alpha}_1}{2}+i\frac{\Delta\bar{n}_1\omega_1}{2c}\right)E_{1x}$$
$$=i\frac{\gamma_e^2\omega_1^2}{2\rho_0c^2v}\frac{1}{(\Omega_{Bxx}-\Omega)-i\frac{\Gamma_B}{2}}E_{1x}E_{2x}^*E_{2x}\frac{1}{2}(1+\mathbf{S}_{x1}\cdot\mathbf{S}_{x2})$$
$$+i\frac{\gamma_e^2\omega_1^2}{2\rho_0c^2v}\frac{1}{(\Omega_{Bxy}-\Omega)-i\frac{\Gamma_B}{2}}E_{1x}E_{2y}^*E_{2y}\frac{1}{2}(1+\mathbf{S}_{x1}\cdot\mathbf{S}_{y2}),\quad(1.1)$$

$$\frac{\partial E_{1y}}{\partial z}+\frac{\bar{n}_1}{c}\frac{\partial E_{1y}}{\partial t}+\left(\bar{\alpha}_1-\frac{\Delta\bar{\alpha}_1}{2}-i\frac{\Delta\bar{n}_1\omega_1}{2c}\right)E_{1y}$$
$$=i\frac{\gamma_e^2\omega_1^2}{2\rho_0c^2v}\frac{1}{(\Omega_{Byy}-\Omega)-i\frac{\Gamma_B}{2}}E_{1y}E_{2y}^*E_{2y}\frac{1}{2}(1+\mathbf{S}_{y1}\cdot\mathbf{S}_{y2})$$
$$+i\frac{\gamma_e^2\omega_1^2}{2\rho_0c^2v}\frac{1}{(\Omega_{Byx}-\Omega)-i\frac{\Gamma_B}{2}}E_{1y}E_{2x}^*E_{2x}\frac{1}{2}(1+\mathbf{S}_{y1}\cdot\mathbf{S}_{x2}),\quad(1.2)$$

$$-\frac{\partial E_{2x}}{\partial z}+\frac{\bar{n}_2}{c}\frac{\partial E_{2x}}{\partial t}+\left(\bar{\alpha}_2+\frac{\Delta\bar{\alpha}_2}{2}+i\frac{\Delta\bar{n}_2\omega_2}{2c}\right)E_{2x}$$
$$=i\frac{\gamma_e^2\omega_2^2}{2\rho_0c^2v}\frac{1}{(\Omega_{Bxx}-\Omega)-i\frac{\Gamma_B}{2}}E_{2x}E_{1x}^*E_{1x}\frac{1}{2}(1+\mathbf{S}_{x1}\cdot\mathbf{S}_{x2})$$
$$+i\frac{\gamma_e^2\omega_2^2}{2\rho_0c^2v}\frac{1}{(\Omega_{Byx}-\Omega)-i\frac{\Gamma_B}{2}}E_{2x}E_{1y}^*E_{1y}\frac{1}{2}(1+\mathbf{S}_{y1}\cdot\mathbf{S}_{x2}),\quad(1.3)$$

$$-\frac{\partial E_{2y}}{\partial z}+\frac{\bar{n}_2}{c}\frac{\partial E_{2y}}{\partial t}+\left(\bar{\alpha}_2-\frac{\Delta\bar{\alpha}_2}{2}-i\frac{\Delta\bar{n}_2\omega_2}{2c}\right)E_{2y}$$
$$=i\frac{\gamma_e^2\omega_2^2}{2\rho_0c^2v}\frac{1}{(\Omega_{Byy}-\Omega)-i\frac{\Gamma_B}{2}}E_{2y}E_{1y}^*E_{1y}\frac{1}{2}(1+\mathbf{S}_{y1}\cdot\mathbf{S}_{y2})$$
$$+i\frac{\gamma_e^2\omega_2^2}{2\rho_0c^2v}\frac{1}{(\Omega_{Bxy}-\Omega)-i\frac{\Gamma_B}{2}}E_{2y}E_{1x}^*E_{1x}\frac{1}{2}(1+\mathbf{S}_{x1}\cdot\mathbf{S}_{y2}).\quad(1.4)$$

Here, $\Omega_{Bxx}=(v/c)(n_{1x}\omega_1+n_{2x}\omega_2)$, $\Omega_{Byy}=(v/c)(n_{1y}\omega_1+n_{2y}\omega_2)$, $\Omega_{Bxy}=(v/c)(n_{1x}\omega_1+n_{2y}\omega_2)$, and $\Omega_{Byx}=(v/c)(n_{1y}\omega_1+n_{2x}\omega_2)$ are the Brillouin frequencies associated with the principal axis beatings [6], where $\omega_1$ is the angular frequency of the PW, and $\omega_2$ is the angular frequency of the SW. $n_{1x}$ and $n_{1y}$, and $n_{2x}$ and $n_{2y}$, are the indices of refraction associated with the principal axes of the PW and SW, respectively. $\Omega$ is the angular frequency of the AW caused by the interaction of the PW and SW. $E_{1x}$ and $E_{1y}$, and $E_{2x}$ and $E_{2y}$, are the complex amplitudes of the PW and the SW, respectively. $c$ is the speed of light, $\rho_0$ is the mean density of the fiber, $\gamma_e$ is the electrostrictive constant, $z$ is the coordinate along the fiber, $v$ is the speed of sound in the fiber, $\Gamma_B$ is the Brillouin linewidth, and finally, $\alpha_{1x}$, $\alpha_{1y}$, $\alpha_{2x}$, and $\alpha_{2y}$ represent the fiber attenuations of the principal axes of polarization of the two interacting waves.

$\boldsymbol{S}_{1x}$, $\boldsymbol{S}_{1y}$, $\boldsymbol{S}_{2x}$, and $\boldsymbol{S}_{2y}$ represent the Stokes vectors in the Poincaré sphere polarization representation [20,21], and are used to define the polarization of the propagating lights [2,20]. Some extra relations of importance are the following:

$\mathbf{S}_{x1} = -\mathbf{S}_{y1}$ for forward propagating light (PW) and $\mathbf{S}_{x2} = -\mathbf{S}_{y2}$ for backward propagating light (SW). Furthermore, it is worthwhile to emphasize that in the above system of Eqs. (1.1)–(1.4), $\mathbf{S}_{x1}$ describes the principal SOP vector for the forward propagating light, and $\mathbf{S}_{x2}$ describes the principal SOP vector of the backward propagating light. In this case, if $\mathbf{S}_{x1}$ is defined as $\mathbf{S}_{x1} = (a, b, c)$, then it must follow that $\mathbf{S}_{y1} = (-a, -b, -c)$, and neglecting the dispersion effect, $\mathbf{S}_{x2} = (a, b, -c)$ and $\mathbf{S}_{y2} = (-a, -b, c)$, where $a$, $b$, and $c$ are the Stokes vector components—the third component, $c$, describing circular birefringence—and are normalized such that $a^2 + b^2 + c^2 = 1$. From this arrangement it is apparent that for fibers having elliptical birefringence ($0 < |c| < 1$), the most general beating situation will be excited; i.e., there will exist four acoustic resonances.

Lastly, the remaining simplifications were introduced to the system of Eqs. (1.1)–(1.4) to make the birefringence effect more explicit. This can be justified by the fact that birefringence and polarization-dependent loss are both small. It is defined $\bar{n}_1 = (n_{1x} + n_{1y})/2$, $\Delta\bar{n}_1 = n_{1x} - n_{1y}$, $\bar{n}_2 = (n_{2x} + n_{2y})/2$, $\Delta\bar{n}_2 = n_{2x} - n_{2y}$ and $\bar{\alpha}_1 = (\alpha_{1x} + \alpha_{1y})/2$, $\Delta\bar{\alpha}_1 = \alpha_{1x} - \alpha_{1y}$, $\bar{\alpha}_2 = (\alpha_{2x} + \alpha_{2y})/2$, $\Delta\bar{\alpha}_2 = \alpha_{2x} - \alpha_{2y}$.

In the above arrangement, the PW input parameters are known only at the beginning of the fiber, i.e., at $z = 0$. Correspondingly, the SW input parameters are known only at the end of the fiber, i.e., at $z = L$, where $L$ is the length of the fiber. Therefore, the boundary conditions for the system of Eqs. (1.1)–(1.4) are similar to previously studied configurations with one pulse [6,22]. The conditions for two pulses are as follows:

$$\begin{aligned} |E_{1x}(0)|^2 &= E_{1x0}^2, \qquad |E_{1y}(0)|^2 = E_{1y0}^2, \\ |E_{2x}(L)|^2 &= E_{2x0}^2, \qquad |E_{2y}(L)|^2 = E_{2y0}^2, \end{aligned} \tag{2}$$

where $E_{1x0}^2$, $E_{1y0}^2$, $E_{2x0}^2$, and $E_{2y0}^2$ are known squared absolute values of the complex fields $E_{1x}$, $E_{1y}$, $E_{2x}$, and $E_{2y}$, respectively. In the dimensionless notation, the system [Eq. (1) becomes

$$\frac{\partial Y_{1x}}{\partial \ell} + \bar{n}_1 \frac{\partial Y_{1x}}{\partial \tau} = -[\beta_{1a} Y_{2x} + \beta_{1b} Y_{2y}] Y_{1x} - \varepsilon_{1x} Y_{1x}, \tag{3.1}$$

$$\frac{\partial Y_{1y}}{\partial \ell} + \bar{n}_1 \frac{\partial Y_{1y}}{\partial \tau} = -[\beta_{1c} Y_{2y} + \beta_{1d} Y_{2x}] Y_{1y} - \varepsilon_{1y} Y_{1y}, \tag{3.2}$$

$$-\frac{\partial Y_{2x}}{\partial \ell} + \bar{n}_2 \frac{\partial Y_{2x}}{\partial \tau} = [\beta_{3a} Y_{1x} + \beta_{3b} Y_{1y}] Y_{2x} - \varepsilon_{2x} Y_{2x}, \tag{3.3}$$

$$-\frac{\partial Y_{2y}}{\partial \ell} + \bar{n}_2 \frac{\partial Y_{2y}}{\partial \tau} = [\beta_{3c} Y_{1y} + \beta_{3d} Y_{1x}] Y_{2y} - \varepsilon_{2y} Y_{2y}, \tag{3.4}$$

$$\beta_{1a} = \frac{4\gamma_e^2 k^2 P_{2x0} L}{r^2 \bar{n}_2 \rho_0 c v \Gamma_B} \cdot \frac{1}{2} \frac{1 + \mathbf{S}_{x1} \cdot \mathbf{S}_{x2}}{1 + \xi_{xx}^2}, \tag{4.1}$$

$$\beta_{1b} = \frac{4\gamma_e^2 k^2 P_{2y0} L}{r^2 \bar{n}_2 \rho_0 c v \Gamma_B} \cdot \frac{1}{2} \frac{1 + \mathbf{S}_{x1} \cdot \mathbf{S}_{y2}}{1 + \xi_{xy}^2}, \tag{4.2}$$

$$\beta_{1c} = \frac{4\gamma_e^2 k^2 P_{2y0} L}{r^2 \bar{n}_2 \rho_0 c v \Gamma_B} \cdot \frac{1}{2} \frac{1 + \mathbf{S}_{y1} \cdot \mathbf{S}_{y2}}{1 + \xi_{yy}^2}, \tag{4.3}$$

$$\beta_{1d} = \frac{4\gamma_e^2 k^2 P_{2x0} L}{r^2 \bar{n}_2 \rho_0 c v \Gamma_B} \cdot \frac{1}{2} \frac{1 + \mathbf{S}_{y1} \cdot \mathbf{S}_{x2}}{1 + \xi_{yx}^2}, \tag{4.4}$$

$$\beta_{3a} = \frac{4\gamma_e^2 k^2 P_{1x0} L}{r^2 \bar{n}_1 \rho_0 c v \Gamma_B} \left(\frac{\omega_2}{\omega_1}\right)^2 \cdot \frac{1}{2} \frac{1 + \mathbf{S}_{x1} \cdot \mathbf{S}_{x2}}{1 + \xi_{xx}^2}, \tag{4.5}$$

$$\beta_{3b} = \frac{4\gamma_e^2 k^2 P_{1y0} L}{r^2 \bar{n}_1 \rho_0 c v \Gamma_B} \left(\frac{\omega_2}{\omega_1}\right)^2 \cdot \frac{1}{2} \frac{1 + \mathbf{S}_{y1} \cdot \mathbf{S}_{x2}}{1 + \xi_{yx}^2}, \tag{4.6}$$

$$\beta_{3c} = \frac{4\gamma_e^2 k^2 P_{1y0} L}{r^2 \bar{n}_1 \rho_0 c v \Gamma_B} \left(\frac{\omega_2}{\omega_1}\right)^2 \cdot \frac{1}{2} \frac{1 + \mathbf{S}_{y1} \cdot \mathbf{S}_{y2}}{1 + \xi_{yy}^2}, \tag{4.7}$$

$$\beta_{3d} = \frac{4\gamma_e^2 k^2 P_{1x0} L}{r^2 \bar{n}_1 \rho_0 c v \Gamma_B} \left(\frac{\omega_2}{\omega_1}\right)^2 \cdot \frac{1}{2} \frac{1 + \mathbf{S}_{x1} \cdot \mathbf{S}_{y2}}{1 + \xi_{xy}^2}. \tag{4.8}$$

In the above system of Eqs. (3.1)–(3.4), we have employed the dimensionless length variable $\ell = z/L$, and the dimensionless time variable $\tau = t/t_c$, where $t_c = L \cdot n_{\text{avg}}/c$ is the transit time, $n_{\text{avg}}$ is the average index of refraction, and $r$ is the radius of the fiber core. The dimensionless intensity variables are defined as the ratio of powers $Y_{1x} = P_{1x}/P_{1x0}$, $Y_{1y} = P_{1y}/P_{1y0}$, $Y_{2x} = P_{2x}/P_{2x0}$, and $Y_{2y} = P_{2y}/P_{2y0}$. Additionally, $\varepsilon_{1x}$, $\varepsilon_{1y}$, $\varepsilon_{2x}$, and $\varepsilon_{2y}$ are the dimensionless loss terms, defined as $\varepsilon_{1x} = 2L\alpha_{1x}$, $\varepsilon_{1y} = 2L\alpha_{1y}$, $\varepsilon_{2x} = 2L\alpha_{2x}$, and $\varepsilon_{2y} = 2L\alpha_{2y}$. The form factor component of the $\beta$ coefficients is defined as $\xi_{ij} = (\Omega_{Bij} - \Omega/(\Gamma_B/2))$, where $i = x, y$ and $j = x, y$. The method of characteristics was employed as in [2,23–25], and the following change of variables was used, where the approximation $\bar{n}_1 \approx \bar{n}_2 = \bar{n}$ was used:

$$u = \frac{1}{\bar{n}}\tau + \ell, \tag{5}$$

$$v = \frac{1}{\bar{n}}\tau - \ell. \tag{6}$$

The resulting system of equations is as follows, with $\beta$ coefficients as defined in expressions (4.1)–(4.8):

$$\frac{dY_{1x}}{du} = -[\beta_{1a} Y_{2x} + \beta_{1b} Y_{2y}] Y_{1x} - \varepsilon_{1x} Y_{1x}, \tag{7.1}$$

$$\frac{dY_{1y}}{du} = -[\beta_{1c} Y_{2y} + \beta_{1d} Y_{2x}] Y_{1y} - \varepsilon_{1y} Y_{1y}, \tag{7.2}$$

$$\frac{dY_{2x}}{dv} = [\beta_{3a} Y_{1x} + \beta_{3b} Y_{1y}] Y_{2x} - \varepsilon_{2x} Y_{2x}, \tag{7.3}$$

$$\frac{dY_{2y}}{dv} = [\beta_{3c}Y_{1y} + \beta_{3d}Y_{1x}]Y_{2y} - \varepsilon_{2y}Y_{2y}. \quad (7.4)$$

The change of variables $u$ and $v$ transforms the system of Eqs. (3.1)–(3.4) of counterpropagating waves into the system of Eqs. (7.1)–(7.4) of copropagating waves. Consequently, we are able to set the following initial conditions:

$$Y_{ij0}(t,0) = [\tanh(a_1(t-b_1))] \cdot [\tanh(-a_2(t-b_2))] + 1, \quad (8)$$

both of which take place at the same end of the new coordinate system, where $i = 1, 2$ and $j = x, y$. The parameters $a_1$ and $a_2$ determine the rise time of the PW and SW pulse profiles, while the parameters $b_1$ and $b_2$ define the center of the pulses.

Though there exist many numerical methods of solution for SBS equations [23,26–31], the fourth-order Runge–Kutta method (RK4) was used to numerically solve the system of Eqs. (7.1)–(7.4), and was chosen for its stability and relatively large step size. Details of this numerical method of solution are summarized in Appendix A.

## 3. RESULTS AND DISCUSSION

Output spectra were calculated by detuning the Stokes frequency, $\omega_2$. Output powers were calculated as $P_{1x\text{-out}} = P_{1x0} \cdot Y_{1x\text{-out}}$, $P_{1y\text{-out}} = P_{1y0} \cdot Y_{1y\text{-out}}$, $P_{2x\text{-out}} = P_{2x0} \cdot Y_{2x\text{-out}}$, and $P_{2y\text{-out}} = P_{2y0} \cdot Y_{2y\text{-out}}$, and the total powers of the PW and the SW were calculated to be $P_1 = P_{1x} + P_{1y}$ and $P_2 = P_{2x} + P_{2y}$, respectively. Also, the attenuation in the fiber has been approximated as $\alpha_{1x} = \alpha_{1y} = \alpha_{2x} = \alpha_{2y} = \alpha = 0.2$ dB/km, and the following parameters of the fiber were used: $n_{\text{avg}} = 1.45$, $\gamma_e = 0.902$, $\lambda = 1550$ nm, $\rho_0 = 2.21$ g/cm$^3$, $v = 5616$ m/s, and $\Gamma_B = 0.1$ GHz. The following indices of refraction will be used to represent the elliptical birefringence, $\Delta n$, of $10^{-4}$, $10^{-5}$, $10^{-6}$, and $10^{-10}$, respectively:

| | |
|---|---|
| $\Delta n = 10^{-4}$ | $\Delta n = 10^{-5}$ |
| $n_{1x} = 1.4508$ | $n_{1x} = 1.45008$ |
| $n_{1y} = 1.4502$ | $n_{1y} = 1.45002$ |
| $n_{2x} = 1.4503$ | $n_{2x} = 1.45003$ |
| $n_{2y} = 1.4504$ | $n_{2y} = 1.45004$ |
| $\Delta n = 10^{-6}$ | $\Delta n = 10^{-10}$ |
| $n_{1x} = 1.450008$ | $n_{1x} = 1.4500000008$ |
| $n_{1y} = 1.450002$ | $n_{1y} = 1.4500000002$ |
| $n_{2x} = 1.450003$ | $n_{2x} = 1.4500000003$ |
| $n_{2y} = 1.450004$ | $n_{2y} = 1.4500000004$ |

### A. Spectral Shift

The appearance of a fast and slow axis results in two optical modes in the fiber with different SBS frequency shifts, causing a mismatch in the corresponding momentum vectors of the AWs, thereby making it impossible for both principal axes to be resonant with the acoustic phonons. The mismatch in phonon resonance causes a Brillouin shift, $\Delta\upsilon_B$, and the larger the birefringence, the larger the Brillouin shift.

Figure 2 shows the magnitude of the Brillouin shift in the output PW and SW spectra.

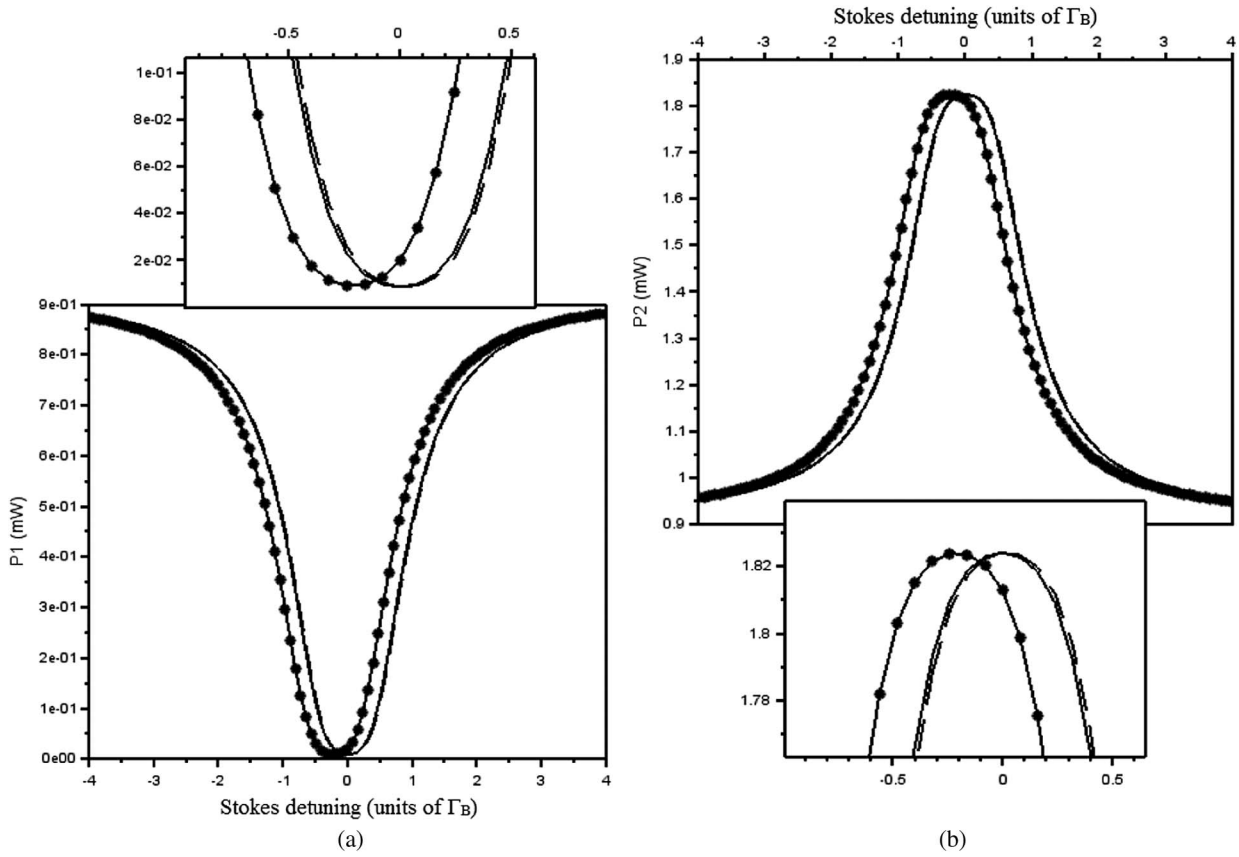


Fig. 2. (a) Output pump spectrum. (b) Output Stokes spectrum. Birefringence $\Delta n$: $*\,10^{-4}$; —$10^{-5}$; - - - $10^{-6}$; LHP(1,0,0); $L = 1000$ m. $P_{1x0} = 0.5$ mW, $P_{1y0} = 0.5$ mW, $P_{2x0} = 0.5$ mW, and $P_{2y0} = 0.5$ mW.

The Brillouin shift, $\Delta\upsilon_B$, was measured as a function of beat length, which is defined in expressions (9) and (10) [6]:

$$L_B = \frac{2\pi}{|(k_{1x} + k_{2x}) - (k_{1y} + k_{2y})|}, \tag{9}$$

where

$$k_{ij} = \frac{n_{ij}}{c}\omega_i, \qquad i = 1, 2, \quad \text{and} \quad j = x, y. \tag{10}$$

Figure 3 summarizes the simulated values of $\Delta\upsilon_B$, in comparison to the beat length for LP light. Two cases were compared for pump and Stokes input powers of 1 mW: (a) the input powers of the $x$ and pump wave components of the PW and the SW were taken to be unequal, and (b) the input powers of the $x$ and $y$ components of the PW and the SW were taken to be equal. From Fig. 3, it is apparent that the degree of birefringence has a nonlinear effect on the Brillouin shift $\Delta\upsilon_B$; in particular, the larger the birefringence, the larger the shift. This spectral shift can in turn be used to quantify the birefringence of the optical fiber upon measurement of the output signal. In addition, the spectral shift appears to be more prominent for unequally balanced input powers of the $x$ and $y$ components of the PW and the SW, as compared to the case of equally balanced powers.

### B. Spectral Distortion

#### *1. Linear Polarization*

The following simulations were performed for LP light. Figure 4 shows the output spectra of the PW and the SW, as well as close-ups of the spectral tips—both of which are linearly horizontally polarized (LHP) in one simulation, and linearly vertically polarized (LVP) in another, the resulting spectra being identical for both LHP and LVP light.

It is often experimentally not possible to achieve a 100% separation of power between the slow and fast modes of the signal. There is power leakage between the $x$ and $y$ axes [32], especially when additional optical components, such a polarization controllers or scramblers [33,34], are used. Hence, for a 11 mW signal, it is a realistic assumption that as much as 1 mW of power could be present in the vertical mode of the signals for LHP light. Likewise, for LVP lights, it is also experimentally plausible to have as much as 1 mW of power in the horizontal mode of the signals.

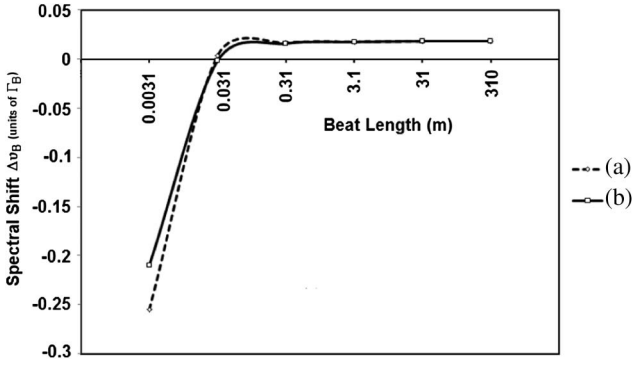


Fig. 3. Brillouin shift dependence on beat length; L = 1000 m, LHP (1,0,0). (a) $P_{1x0} = 0.9$ mW, $P_{1y0} = 0.1$ mW, $P_{2x0} = 0.9$ mW, and $P_{2y0} = 0.1$ mW. (b) $P_{1x0} = 0.5$ mW, $P_{1y0} = 0.5$ mW, $P_{2x0} = 0.5$ mW, and $P_{2y0} = 0.5$ mW.

The shape of the output spectra in Fig. 4 can be explained by the modified interaction between the PW and the SW during LP. Referring to the system of Eqs. (7.1)–(7.4) and $\beta$ coefficients (4.1)–(4.3), (4.8), we see that the $\beta$ coefficients $\beta_{1b}$, $\beta_{1d}$, $\beta_{3b}$, and $\beta_{3d}$ are reduced to zero for both LHP and LVP light. As a result, the system [Eq. (7) is broken up into two smaller systems consisting of (a) Eqs. (7.1) and (7.3) and (b) Eqs. (7.2) and (7.4), respectively, which are independent of each other. The first system describes the interaction between the horizontal components ($x$ components) of the PW and the SW, and the second system describes the interaction between the vertical components ($y$ components) of the PW and the SW. In other words, interactions along the $x$ and $y$ components become independent from each other, which is to be expected during linear polarization.

In Fig. 4, which shows the output pump and Stokes spectra of LHP light for various pulse lengths, the little "blip" at the bottom/top of the spectra is the $y$-component contribution, while the "general" shape of the spectra is a result of the $x$-component contribution. Since the power in the horizontal mode is large for LHP light, the resultant depletion of the PW and amplification of the SW are also large, leading to the general trend of the output spectra in Fig. 4. This is the spectral shape that would be expected for an idealized LHP light (or perhaps light with no consideration for polarization at all). However, the LHP is not ideal, and there exists a small interaction in the vertical component. Since the power along the $y$ axis is small, the resultant contribution is also small. As can be seen from Fig. 4, the smaller the power in the $y$ component, the smaller the contribution, and the weaker the spectral distortion of the graph. In other words, increasing powers in the $y$ components increase the degree of spectral distortion. For $P_{1y} = P_{2y} = 1$ mW, the spectral "blip" is much larger than for the case in which $P_{1y} = P_{2y} = 0.1$ mW, which is practically nonexistent. However, while a smaller power leakage causes a smaller spectral distortion or "blip", it yields output spectra with a larger depletion, or "flat-top," than in the case of larger power leakage. For the steady-state regime, shown in Figs. 4(a) and 4(b), where both the PW and the SW are continuous waves, the "flat-top" effect is more prominent, and the spectral "blip" is less pronounced, as compared to shorter pulse lengths of 240 and 79 ns, shown in Figs. 4(c) and 4(d) and Figs. 4(e) and 4(f), respectively. With decreasing temporal pulsewidth, the power leakage causes the distorted spectral tip to be sharper and more pronounced, as compared to longer pulses.

For sensing applications, it is detrimental to have a depleted spectrum [7–9], since depletion and spectral flattening make it difficult to accurately measure the center frequency of the spectrum. Although the distorted spectra with smaller depletion, obtained from the steady-state interaction of the PW and the SW, may not have a sufficiently prominent spectral tip for sensing applications, it is an improvement nonetheless, as compared to the case of larger depletion, in which the "flat-top" spans an even larger frequency range.

As shown in Figs. 4(e) and 4(f), a shorter pulse length of 79 ns undergoing spectral leakage between the fast and slow modes has a sufficiently prominent spectral tip for measurement in sensing applications. As such, by using the distortion effects caused by birefringence to our advantage, it is possible to provide a regime that is favorable for sensing applications

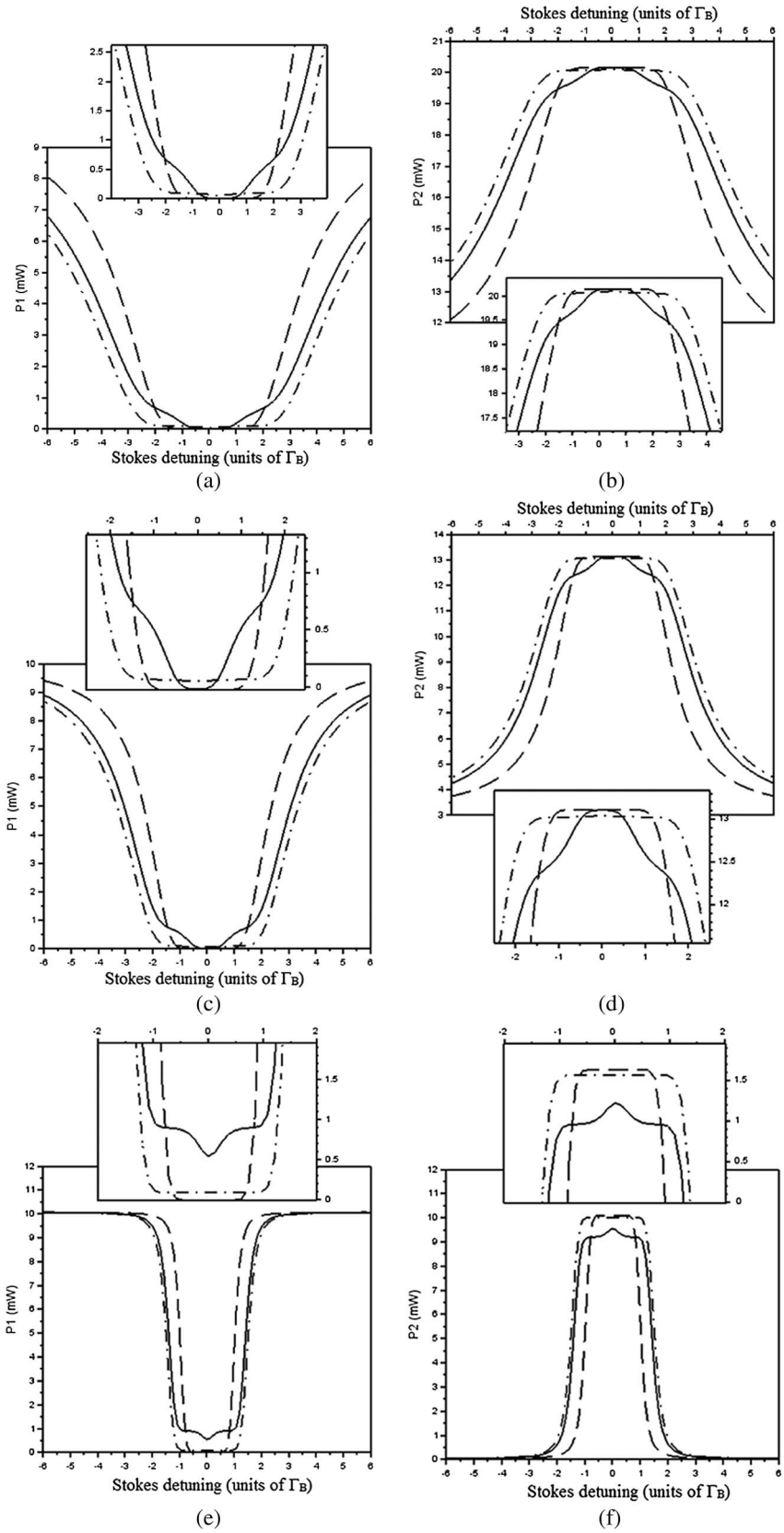


Fig. 4. Left: output pump spectrum. Right: output Stokes spectrum. (a), (b) steady state; (c), (d) 240 ns pulse; (e), (f) 79 ns pulse; birefringence $\Delta n = 10^{-4}$, L = 1 km. –·–·–: $P_{1x0} = 10.0$ mW, $P_{1y0} = 1.0$ mW, $P_{2x0} = 10.0$ mW, and $P_{2y0} = 1.0$ mW; LHP (1,0,0). —: $P_{1x0} = 10.9$ mW, $P_{1y0} = 0.1$ mW, $P_{2x0} = 10.9$ mW, and $P_{2y0} = 0.1$ mW; LHP (1,0,0). - - -: $P_{1x0} = 10.0$ mW, $P_{1y0} = 1.0$ mW, $P_{2x0} = 10.0$ mW, and $P_{2y0} = 1.0$ mW; no pol (0,0,0).

related to SBS, by increasing the power leakage between the fast and slow modes, as well as decreasing the pulse length during LP.

In the case of LVP, also shown in Fig. 4, the roles of the $x$ and $y$ components are reversed, but the interaction is identical. For this reason, the two cases of LHP and LVP light, shown in Fig. 4, give identical results, as in either case, the interaction along the slow or fast axes remains the same.

Also, in Fig. 4, the output spectra of LP light for all pulse lengths are shown in comparison to light without a dependence on polarization, depicted by the dashed line—namely, light having a Stokes vector $\boldsymbol{S} = (0, 0, 0)$, which has been taken to be a first-order approximation to truly unpolarized light. The spectra of the LP are spread out in the frequency domain, as compared to nonpolarized light in a nonbirefringent fiber. This effect can be explained by the nature of the LP interaction between the PW and the SW. As discussed above, when LP is not ideal, there exists a small independent interaction along either the fast or the slow mode, contributing to the spectral distortion. The interaction along the main axis of polarization, however, contributes the most to the output spectral shape of the light—the SOP of the counterpropagating waves being lined up for maximum gain [3,11,12,14,16,17]. Additionally, since this interaction is strong, and the input powers along the main mode are comparatively large, the output light experiences a significant gain/depletion, causing the spectrum itself to be larger and inherently spread out [9]. This effect does not present itself for unpolarized light, where there cannot be polarization alignment for maximum gain. All four lights interact with each other, and as a result, the output spectrum is smaller, which contributes to less spectral spreading in the frequency domain.

As a result, the model presented for LP light proves to be a valuable measure of the experimentally realistic case of nonideal LP light in optical fibers, or a measure of power leakage between the fast and slow modes. The degree of spectral distortion may be used as an indication of the quality of LP during the SBS interaction.

### 2. Elliptical Polarization for Steady-State Interaction

In this section, the continuous PW and SW were simulated to have several elliptical polarizations: Random 1 (0.1, 0.9, 0.42), Random 2 (0.3, 0.7, 0.65), Random 3 (0.58, 0.58, 0.58), and Random 4 (0.1, 0.9, 0.42). The effect of elliptical polarization on the spectral shape of the output light was observed for pump and Stokes input powers: (a) below the Brillouin threshold and (b) above the Brillouin threshold [1,2].

In Fig. 5, the individual $x$ and $y$ components of the SW have been plotted. Moderate powers have been chosen for various degrees of birefringence: $10^{-4}$, $10^{-5}$, and $10^{-6}$. It can be seen that the spectral distortion that results due to the birefringence is more prominent for higher degrees of birefringence ($10^{-4}$) as compared to lower degrees of birefringence ($10^{-6}$).

In the most general case of elliptical birefringence, there are four running AWs, each having its own resonance frequency. As a result, each of the fast and slow modes has its own resonant frequency, which is the cause of the multiple peaks on the output spectra in Fig. 5.

In Figs. 6 and 7, input powers have been taken beyond the Brillouin threshold for various elliptical polarizations. It can be seen that certain polarizations cause a kind of spectral hole burning effect [35,36] to take place in the output spectrum, while others affect the spectral shape negligibly.

In Fig. 6, for example, the spectral hole burning effect can be explained as a result of a very strong interaction along one mode of the optical fiber, and weak interactions along the other modes for the polarization Random 4 (0.1, 0.9, 0.42). In Fig. 6, since the input power of the Stokes $y$ component

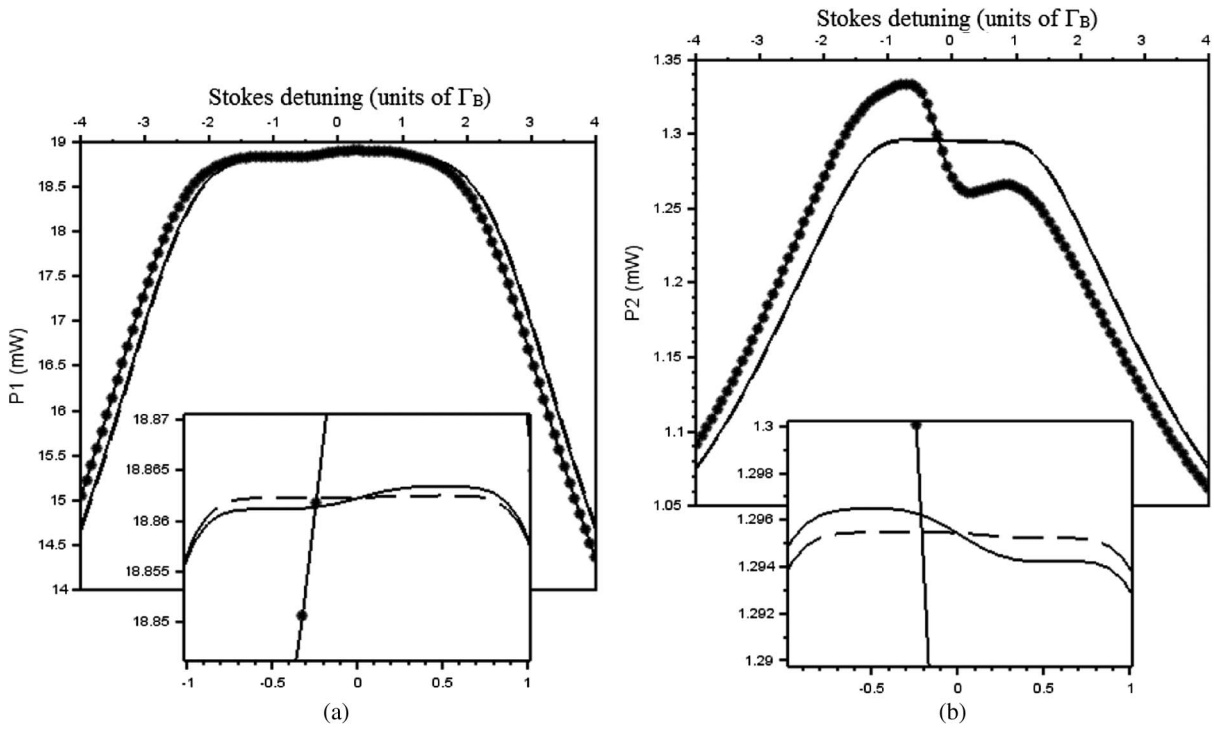


Fig. 5. (a) $x$ component of output Stokes spectrum. (b) $y$ component of output Stokes spectrum. Birefringence $\Delta n$: $*\,10^{-4}$; —$10^{-5}$; - - -$10^{-6}$; Random4 (0.1,0.9,0.42), $L = 1000$ m. $P_{1x0} = 10.0$ mW, $P_{1y0} = 1.0$ mW, $P_{2x0} = 10.0$ mW, and $P_{2y0} = 1.0$ mW.

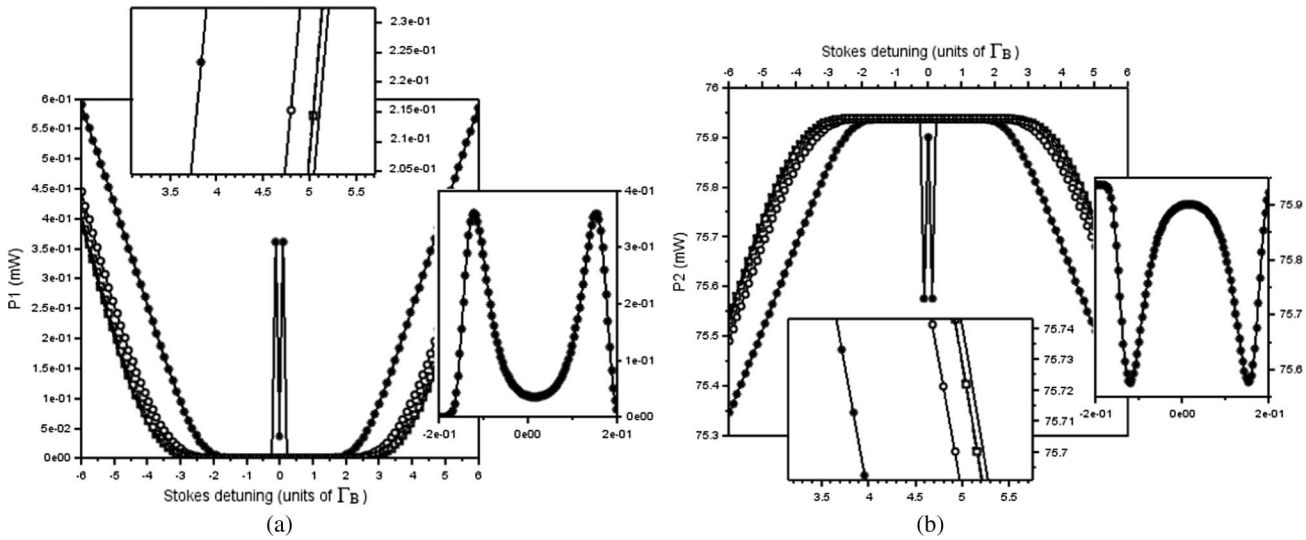


(a) (b)

Fig. 6. (a) Output pump spectrum. (b) Output Stokes spectrum. Birefringence $\Delta n$: □ $10^{-6}$ Random 1 (0.6, 0.25, 0.76); - - -$10^{-6}$ Random 2 (0.3, 0.7, 0.65); $L = 1000$ m ◯ $10^{-6}$ Random 3 (0.58, 0.58, 0.58); * $10^{-6}$ Random 4 (0.1, 0.9,0.42); —$10^{-10}$ no pol (0,0,0). $P_{1x0} = 1.0$ mW, $P_{1y0} = 1.0$ mW, $P_{2x0} = 1.0$ mW, and $P_{2y0} = 80.0$ mW

is so large (80 mW), and the corresponding vertical polarization component is also large (0.9), it acts to quickly deplete power from the other modes, and since, as mentioned previously, there is no single resonant frequency, it does so along multiple resonant frequencies. For polarizations Random 1 (0.6, 0.25, 0.76), Random 2 (0.3, 0.7, 0.65), and Random 3 (0.3, 0.7, 0.65), the combination of the relatively weak vertical polarization component and the strong circular polarization component almost eliminates the effect altogether. Polarizations Random 1 and Random 2 are nearly identical to the nonpolarized light; hence these polarizations can be used to maintain the fidelity of the spectral shape to be as close as possible to nonpolarized light, which is unaffected by birefringence. Additionally, the effects of distortion on the FWHM of the output pulse can be minimized, which has numerous applications in communications and data transmission.

A similar general spectral broadening effect can be observed in Fig. 7, though because of the different power distribution among the modes there is no longer a spectral hole burning effect. In addition, polarizations Random 1, Random 2, and Random 3 are no longer nearly identical to the unpolarized light, due to the different interactions between the four lights caused by varied initial power distributions.

As a result, it has been shown that elliptical birefringence has a prominent effect on the spectral shape of the output PW

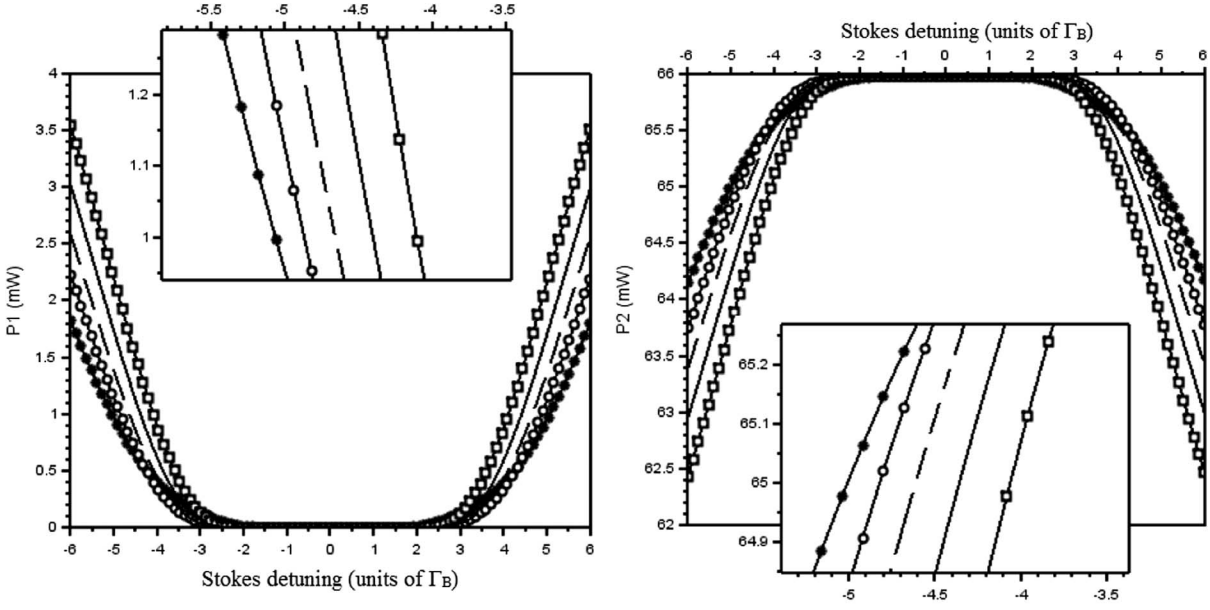


(a) (b)

Fig. 7. (a) Output pump spectrum. (b) Output Stokes spectrum. Birefringence $\Delta n$: □ $10^{-6}$ Random 1 (0.6, 0.25, 0.76); - - -$10^{-6}$ Random 2 (0.3, 0.7, 0.65); $L = 1000$ m ◯ $10^{-6}$ Random 3 (0.58, 0.58, 0.58); * $10^{-6}$ Random 4 (0.1, 0.9,0.42); —$10^{-10}$ no pol (0,0,0). $P_{1x0} = 10.0$ mW, $P_{1y0} = 1.0$ mW, $P_{2x0} = 60.0$ mW, and $P_{2y0} = 1.0$ mW.

and SW. In some cases, it causes a spectral hole burning effect as well as spectral spreading, while in other cases it is possible to choose a polarization and power combination to minimize the spectral distortion of the FWHM of the output pulse, and maintain pulse fidelity.

## 4. CONCLUSION

In summary, it has been observed that the degree of birefringence, or beat length, is responsible for an observed Brillouin shift, $\Delta v_B$, in the output PW and SW spectra. Polarization and elliptical birefringence have a prominent effect on the spectral shape of output light—in particular, nonideal LP light causes spectral distortion, which appears in the shape of a "blip" on top of the expected spectral shape, as well as spreading of the spectrum in the frequency domain. As such, a good measure for detecting nonideal LP light has been established. Additionally, due to the smaller spectral depletion of the nonideal LP light, which is preferable for sensing applications, a regime that is preferable for measurement in sensing applications has been proposed. Elliptical polarization and birefringence, for moderate input powers of the PW and the SW, also cause the spectrum to spread out in the frequency domain. For high input powers, a spectral hole burning effect is predicted for certain elliptical polarizations. Other elliptical polarizations provide means for maintaining the FWHM and pulse fidelity of the Brillouin spectral shape—even for powers beyond the Brillouin threshold.

## APPENDIX A

### 1. Derivation of the System of Eqs (1.1)–(1.4)

Let us consider the simple case of two propagation constants in the fiber, calling them $\hat{\mathrm{x}}$ and $\hat{\mathrm{y}}$ for now. If a light with an angular frequency $\omega$ was injected in the fiber, the electric fields could be written in the following form, in terms of their principal axis of polarization:

$$|E_1(z,t)\rangle = E_x \exp\{i[k_x z - \omega t]\}|\hat{\mathrm{x}}\rangle + E_y \exp\{i[k_y z - \omega t]\}|\hat{\mathrm{y}}\rangle. \tag{A1}$$

We have $\langle\hat{\mathrm{x}}|\hat{\mathrm{x}}\rangle = 1 = \langle\hat{\mathrm{y}}|\hat{\mathrm{y}}\rangle$ and $\langle\hat{\mathrm{x}}|\hat{\mathrm{y}}\rangle = 0$. Considering two counterpropagating beams in the fiber, we can individually write them for the positive $z$-propagating light,

$$\begin{aligned}|E_1(z,t)\rangle = {} & E_{1x} \exp\{i[k_{1x} z - \omega_1 t]\}|\hat{\mathrm{x}}_1\rangle \\ & + E_{1y} \exp\{i[k_{1y} z - \omega_1 t]\}|\hat{\mathrm{y}}_1\rangle,\end{aligned} \tag{A2}$$

and the negative $z$-propagating light,

$$\begin{aligned}|E_2(z,t)\rangle = {} & E_{2x} \exp\{i[-k_{2x} z - \omega_2 t]\}|\hat{\mathrm{x}}_2\rangle \\ & + E_{2y} \exp\{i[k_{2y} z - \omega_2 t]\}|\hat{\mathrm{y}}_2\rangle.\end{aligned} \tag{A3}$$

The beating via electrostriction in the fiber due to the two light waves can be written explicitly:

$$\begin{aligned}&\langle E_2(z,t)|E_1(z,t)\rangle \\ &\quad = E_{1x}E_{2x}^* \exp\{i[(k_{1x}+k_{2x})z - (\omega_1-\omega_2)t]\}\langle\hat{\mathrm{x}}_2|\hat{\mathrm{x}}_1\rangle \\ &\qquad + E_{1y}E_{2y}^* \exp\{i[(k_{1y}+k_{2y})z - (\omega_1-\omega_2)t]\}\langle\hat{\mathrm{y}}_2|\hat{\mathrm{y}}_1\rangle \\ &\qquad + E_{1x}E_{2y}^* \exp\{i[(k_{1x}+k_{2y})z - (\omega_1-\omega_2)t]\}\langle\hat{\mathrm{y}}_2|\hat{\mathrm{x}}_1\rangle \\ &\qquad + E_{1y}E_{2x}^* \exp\{i[(k_{1y}+k_{2x})z - (\omega_1-\omega_2)t]\}\langle\hat{\mathrm{x}}_2|\hat{\mathrm{y}}_1\rangle.\end{aligned} \tag{A4}$$

In the most general case of elliptical birefringence, we will have $\langle\hat{\mathrm{x}}_2|\hat{\mathrm{x}}_1\rangle \neq 1 \neq \langle\hat{\mathrm{y}}_2|\hat{\mathrm{y}}_1\rangle$ and furthermore $\langle\hat{\mathrm{y}}_2|\hat{\mathrm{x}}_1\rangle \neq 0 \neq \langle\hat{\mathrm{x}}_2|\hat{\mathrm{y}}_1\rangle$. The direct physical consequence of this is that there are now four acoustic running waves.

Taking the steady-state approximation, we have the complex acoustic field amplitude for the simplest case of zero birefringence:

$$\Delta\rho = \frac{\gamma_e q^q}{\Omega_B^2 - \Omega^2 - i\Gamma_B\Omega}\langle E_2(z,t)|E_1(z,t)\rangle \tag{A5}$$

To generalize the result to the case of elliptical birefringence, where it is expected to have the corresponding resonance frequency associated with the principal birefringence axes, we make $\Omega_B$ functions of the polarization principal axis beatings [6]. Using the approximation $q = k_1 + k_2 = \frac{1}{c}(n_1\omega_1 + n_2\omega_2) \cong 2(\bar{n}\,\bar{\omega}/c)$, where $\bar{n}$ and are taken to be the averages of $n_1$ and $n_2$, and $\omega_1$ and $\omega_2$, respectively, it is then possible to have the following approximate complex acoustic field amplitudes,

$$\begin{aligned}\Delta\rho = {} & \frac{\gamma_e\bar{n}\,\bar{\omega}}{cv}\frac{1}{(\Omega_{Bxx}-\Omega) - i\frac{\Gamma_B}{2}}E_{1x}E_{2x}^* \exp\{i[(k_{1x}+k_{2x})z \\ & - (\omega_1-\omega_2)t]\}\langle\hat{\mathrm{x}}_2|\hat{\mathrm{x}}_1\rangle \\ & + \frac{\gamma_e\bar{n}\,\bar{\omega}}{cv}\frac{1}{(\Omega_{Byy}-\Omega) - i\frac{\Gamma_B}{2}}E_{1y}E_{2y}^* \exp\{i[(k_{1y}+k_{2y})z \\ & - (\omega_1-\omega_2)t]\}\langle\hat{\mathrm{y}}_2|\hat{\mathrm{y}}_1\rangle \\ & + \frac{\gamma_e\bar{n}\,\bar{\omega}}{cv}\frac{1}{(\Omega_{Bxy}-\Omega) - i\frac{\Gamma_B}{2}}E_{1x}E_{2y}^* \exp\{i[(k_{1x}+k_{2y})z \\ & - (\omega_1-\omega_2)t]\}\langle\hat{\mathrm{y}}_2|\hat{\mathrm{x}}_1\rangle \\ & + \frac{\gamma_e\bar{n}\,\bar{\omega}}{cv}\frac{1}{(\Omega_{Byx}-\Omega) - i\frac{\Gamma_B}{2}}E_{1y}E_{2x}^* \exp\{i[(k_{1y}+k_{2x})z \\ & - (\omega_1-\omega_2)t]\}\langle\hat{\mathrm{x}}_2|\hat{\mathrm{y}}_1\rangle.\end{aligned} \tag{A6}$$

Paying attention to the original case without birefringence in Eq. (A5), it is possible to generalize our result. Recall that nonbirefringent lights were assumed to undergo ideal power transfer between the PW and the SW, as would be the case when both of these waves are parallel polarized (under the slowly varying amplitudes, $A_1$ and $A_2$, approximation),

$$\frac{\partial A_1}{\partial z} + \frac{n}{c}\frac{\partial A_1}{\partial t} + \alpha A_1 = i\frac{\gamma_e\omega_1}{2\rho_0 nc}\Delta\rho\cdot A_2 \tag{A7.1}$$

$$-\frac{\partial A_2}{\partial z} + \frac{n}{c}\frac{\partial A_2}{\partial t} + \alpha A_2 = i\frac{\gamma_e\omega_2}{2\rho_0 nc}\Delta\rho^*\cdot A_1. \tag{A7.2}$$

In Eqs. (A7.1) and (A7.2), $\rho_0$ is the mean density of the fiber. Generalizing the above system of Eq. (A7) to the case of birefringence we take the following:

$$\frac{\partial E_{1x}}{\partial z}+\frac{n_{1x}}{c}\frac{\partial E_{1x}}{\partial t}+\alpha_{1x}E_{1x}$$
$$=i\frac{\gamma_e\omega_1}{2\rho_0 n_{1x}c}\frac{\gamma_e\bar{n}\bar{\omega}}{cv}\frac{1}{(\Omega_{Bxx}-\Omega)-i\frac{\Gamma_B}{2}}E_{1x}E_{2x}^{*}E_{2x}\langle\widehat{\mathrm{x}}_2|\widehat{\mathrm{x}}_1\rangle\langle\widehat{\mathrm{x}}_1|\widehat{\mathrm{x}}_2\rangle$$
$$+i\frac{\gamma_e\omega_1}{2\rho_0 n_{1x}c}\frac{\gamma_e\bar{n}\bar{\omega}}{cv}\frac{1}{(\Omega_{Bxy}-\Omega)-i\frac{\Gamma_B}{2}}E_{1x}E_{2y}^{*}E_{2y}\langle\widehat{\mathrm{y}}_2|\widehat{\mathrm{x}}_1\rangle\langle\widehat{\mathrm{x}}_1|\widehat{\mathrm{y}}_2\rangle, \tag{A8.1}$$

$$\frac{\partial E_{1y}}{\partial z}+\frac{n_{1y}}{c}\frac{\partial E_{1y}}{\partial t}+\alpha_{1y}E_{1y}$$
$$=i\frac{\gamma_e\omega_1}{2\rho_0 n_{1y}c}\frac{\gamma_e\bar{n}\bar{\omega}}{cv}\frac{1}{(\Omega_{Byy}-\Omega)-i\frac{\Gamma_B}{2}}E_{1y}E_{2y}^{*}E_{2y}\langle\widehat{\mathrm{y}}_2|\widehat{\mathrm{y}}_1\rangle\langle\widehat{\mathrm{y}}_1|\widehat{\mathrm{y}}_2\rangle$$
$$+i\frac{\gamma_e\omega_1}{2\rho_0 n_{1y}c}\frac{\gamma_e\bar{n}\bar{\omega}}{cv}\frac{1}{(\Omega_{Byx}-\Omega)-i\frac{\Gamma_B}{2}}$$
$$\times E_{1y}E_{2x}^{*}E_{2x}\langle\widehat{\mathrm{x}}_2|\widehat{\mathrm{y}}_1\rangle\langle\widehat{\mathrm{y}}_1|\widehat{\mathrm{x}}_2\rangle, \tag{A8.2}$$

$$-\frac{\partial E_{2x}}{\partial z}+\frac{n_{2x}}{c}\frac{\partial E_{2x}}{\partial t}+\alpha_{2x}E_{2x}$$
$$=i\frac{\gamma_e\omega_2}{2\rho_0 n_{2x}c}\frac{\gamma_e\bar{n}\bar{\omega}}{cv}\frac{1}{(\Omega_{Bxx}-\Omega)-i\frac{\Gamma_B}{2}}E_{2x}E_{1x}^{*}E_{1x}\langle\widehat{\mathrm{x}}_1|\widehat{\mathrm{x}}_2\rangle\langle\widehat{\mathrm{x}}_2|\widehat{\mathrm{x}}_1\rangle$$
$$+i\frac{\gamma_e\omega_2}{2\rho_0 n_{2x}c}\frac{\gamma_e\bar{n}\bar{\omega}}{cv}\frac{1}{(\Omega_{Byx}-\Omega)-i\frac{\Gamma_B}{2}}E_{2x}E_{1y}^{*}E_{1y}\langle\widehat{\mathrm{y}}_1|\widehat{\mathrm{x}}_2\rangle\langle\widehat{\mathrm{x}}_2|\widehat{\mathrm{y}}_1\rangle, \tag{A8.3}$$

$$-\frac{\partial E_{2y}}{\partial z}+\frac{n_{2y}}{c}\frac{\partial E_{2y}}{\partial t}+\alpha_{2y}E_{2y}$$
$$=i\frac{\gamma_e\omega_2}{2\rho_0 n_{2y}c}\frac{\gamma_e\bar{n}\bar{\omega}}{cv}\frac{1}{(\Omega_{Byy}-\Omega)-i\frac{\Gamma_B}{2}}E_{2y}E_{1y}^{*}E_{1y}\langle\widehat{\mathrm{y}}_1|\widehat{\mathrm{y}}_2\rangle\langle\widehat{\mathrm{y}}_2|\widehat{\mathrm{y}}_1\rangle$$
$$+i\frac{\gamma_e\omega_2}{2\rho_0 n_{2y}c}\frac{\gamma_e\bar{n}\bar{\omega}}{cv}\frac{1}{(\Omega_{Bxy}-\Omega)-i\frac{\Gamma_B}{2}}E_{2y}E_{1x}^{*}E_{1x}\langle\widehat{\mathrm{y}}_2|\widehat{\mathrm{x}}_1\rangle\langle\widehat{\mathrm{x}}_1|\widehat{\mathrm{y}}_2\rangle. \tag{A8.4}$$

The attenuations $\alpha_{1x}$, $\alpha_{1y}$, $\alpha_{2x}$, and $\alpha_{2y}$ represent the fiber attenuations of the principal axes of polarizations $|\widehat{\mathrm{x}}_1\rangle$, $|\widehat{\mathrm{y}}_1\rangle$, $|\widehat{\mathrm{x}}_2\rangle$, and $|\widehat{\mathrm{y}}_2\rangle$, respectively. Finally, using the identity $|\widehat{\mathrm{x}}\rangle\langle\widehat{\mathrm{x}}|=\frac{1}{2}(1+\mathbf{S}_x\cdot\boldsymbol{\sigma})$, which links the Jones matrix unit vector to its Stokes vector $\mathbf{S}_x$ on the Poincaré sphere via the Pauli matrix $\boldsymbol{\sigma}$, as well as the simplifications for $\bar{n}_1$, $\Delta\bar{n}_1$, $\bar{n}_2$, $\Delta\bar{n}_2$, $\bar{\alpha}_1$, $\Delta\bar{\alpha}_1$, $\bar{\alpha}_2$, and $\Delta\bar{\alpha}_2$, we arrive at the system of Eq. (1).

## 2. Fourth-Order Runge–Kutta Method of Solution

Using the RK4 numerical method, the solution of $\bar{\alpha}_1$ system (7) is summarized in Eqs. (A9.1)–(A9.4), where $n$ is the temporal step, and $j$ is the spatial step:

$$Y_{1x}(n+1,j+1)=Y_{1x}(n,j)+\frac{K_1+2K_2+2K_3+K_4}{6}, \tag{A9.1}$$

$$Y_{1y}(n+1,j+1)=Y_{1y}(n,j)+\frac{L_1+2L_2+2L_3+L_4}{6}, \tag{A9.2}$$

$$Y_{2x}(n+1,j+1)=Y_{2x}(n,j)+\frac{Q_1+2Q_2+2Q_3+Q_4}{6}, \tag{A9.3}$$

$$Y_{2y}(n+1,j+1)=Y_{2y}(n,j)+\frac{R_1+2R_2+2R_3+R_4}{6}, \tag{A9.4}$$

where the coefficients $K_i$, $L_i$, $Q_i$, and $R_i$, where $i=1,2,3,4$, are defined as

$$K_1=-\lfloor\beta_{1a}Y_{2x}(n,j)+\beta_{1b}Y_{2y}(n,j)+\varepsilon_{1x}\rfloor\cdot Y_{1x}(n,j)\cdot\Delta u, \tag{A10.1}$$

$$L_1=-\lfloor\beta_{1c}Y_{2y}(n,j)+\beta_{1d}Y_{2x}(n,j)+\varepsilon_{1y}\rfloor\cdot Y_{1y}(n,j)\cdot\Delta u, \tag{A10.2}$$

$$Q_1=\lfloor\beta_{3a}Y_{1x}(n,j)+\beta_{3b}Y_{1y}(n,j)+\varepsilon_{2x}\rfloor\cdot Y_{2x}(n,j)\cdot\Delta v, \tag{A10.3}$$

$$R_1=\lfloor\beta_{3c}Y_{1y}(n,j)+\beta_{3d}Y_{1x}(n,j)+\varepsilon_{2y}\rfloor\cdot Y_{2y}(n,j)\cdot\Delta v, \tag{A10.4}$$

$$K_2=-\left[\beta_{1a}\left[Y_{2x}(n,j)+\frac{Q_1}{2}\right]+\beta_{1b}\left[Y_{2y}(n,j)+\frac{R_1}{2}\right]+\varepsilon_{1x}\right]\cdot\left[Y_{1x}(n,j)+\frac{K_1}{2}\right]\cdot\Delta u, \tag{A11.1}$$

$$L_2=-\left[\beta_{1c}\left[Y_{2y}(n,j)+\frac{R_1}{2}\right]+\beta_{1d}\left[Y_{2x}(n,j)+\frac{Q_1}{2}\right]+\varepsilon_{1y}\right]\cdot\left[Y_{1y}(n,j)+\frac{L_1}{2}\right]\cdot\Delta u, \tag{A11.2}$$

$$Q_2=\left[\beta_{3a}\left[Y_{1x}(n,j)+\frac{K_1}{2}\right]+\beta_{3b}\left[Y_{1y}(n,j)+\frac{L_1}{2}\right]+\varepsilon_{2x}\right]\cdot\left[Y_{2x}(n,j)+\frac{Q_1}{2}\right]\cdot\Delta v, \tag{A11.3}$$

$$R_2=\left[\beta_{3c}\left[Y_{1y}(n,j)+\frac{L_1}{2}\right]+\beta_{3d}\left[Y_{1x}(n,j)+\frac{K_1}{2}\right]+\varepsilon_{2y}\right]\cdot\left[Y_{2y}(n,j)+\frac{R_1}{2}\right]\cdot\Delta v, \tag{A11.4}$$

$$K_3=-\left[\beta_{1a}\left[Y_{2x}(n,j)+\frac{Q_2}{2}\right]+\beta_{1b}\left[Y_{2y}(n,j)+\frac{R_2}{2}\right]+\varepsilon_{1x}\right]\cdot\left[Y_{1x}(n,j)+\frac{K_2}{2}\right]\cdot\Delta u, \tag{A12.1}$$

$$L_3 = -\left[\beta_{1c}\left[Y_{2y}(n,j)+\frac{R_2}{2}\right]+\beta_{1d}\left[Y_{2x}(n,j)+\frac{Q_2}{2}\right]+\varepsilon_{1y}\right] \cdot \left[Y_{1y}(n,j)+\frac{L_2}{2}\right]\cdot \Delta u, \tag{A12.2}$$

$$Q_3 = \left[\beta_{3a}\left[Y_{1x}(n,j)+\frac{K_2}{2}\right]+\beta_{3b}\left[Y_{1y}(n,j)+\frac{L_2}{2}\right]+\varepsilon_{2x}\right] \cdot \left[Y_{2x}(n,j)+\frac{Q_2}{2}\right]\cdot \Delta v, \tag{A12.3}$$

$$R_3 = \left[\beta_{3c}\left[Y_{1y}(n,j)+\frac{L_2}{2}\right]+\beta_{3d}\left[Y_{1x}(n,j)+\frac{K_2}{2}\right]+\varepsilon_{2y}\right] \cdot \left[Y_{2y}(n,j)+\frac{R_2}{2}\right]\cdot \Delta v, \tag{A12.4}$$

$$K_4 = -\lfloor \beta_{1a}\lfloor Y_{2x}(n,j)+Q_3\rfloor+\beta_{1b}\lfloor Y_{2y}(n,j)+R_3\rfloor+\varepsilon_{1x}\rfloor \cdot \lfloor Y_{1x}(n,j)+K_3\rfloor\cdot \Delta u, \tag{A13.1}$$

$$L_4 = -\lfloor \beta_{1c}\lfloor Y_{2y}(n,j)+R_3\rfloor+\beta_{1d}\lfloor Y_{2x}(n,j)+Q_3\rfloor+\varepsilon_{1y}\rfloor \cdot \lfloor Y_{1y}(n,j)+L_3\rfloor\cdot \Delta u, \tag{A13.2}$$

$$Q_4 = \lfloor \beta_{3a}\lfloor Y_{1x}(n,j)+K_3\rfloor+\beta_{3b}\lfloor Y_{1y}(n,j)+L_3\rfloor+\varepsilon_{2x}\rfloor \cdot \lfloor Y_{2x}(n,j)+Q_3\rfloor\cdot \Delta v, \tag{A13.3}$$

$$R_4 = \lfloor \beta_{3c}\lfloor Y_{1y}(n,j)+L_3\rfloor+\beta_{3d}\lfloor Y_{1x}(n,j)+K_3\rfloor+\varepsilon_{2y}\rfloor \cdot \lfloor Y_{2y}(n,j)+R_3\rfloor\cdot \Delta v. \tag{A13.4}$$

## REFERENCES


1. R. Boyd, *Nonlinear Optics* (Academic, 1992).
2. G. P. Agrawal, *Nonlinear Fiber Optics* (Academic, 2006).
3. R. H. Stolen, "Polarization effects in fiber Raman and Brillouin lasers," IEEE J. Quantum Electron. **QE-15**, 1157–1160 (1979).
4. D. R. Walker, M. Bashkanski, A. Gulian, F. K. Fatemi, and M. Steiner, "Stabilizing slow light delay in stimulated Brillouin scattering using a Faraday rotator mirror," J. Opt. Soc. Am. B **25**, C61–C64 (2008).
5. O. Shlomovits and M. Tur, "Vector analysis of depleted stimulated Brillouin scattering amplification in standard single-mode fibers with non-zero birefringence," Opt. Lett. **38**, 836–838 (2013).
6. X. Bao and L. Chen, "Recent progress in Brillouin scattering based fiber sensors," Sensors **11**, 4152–4187 (2011).
7. F. Ravet, *Performance of the Distributed Brillouin Sensor: Benefits and Penalties Due to Pump Depletion* (University of Ottawa, 2007).
8. T. Horiguchi, K. Shimizu, T. Kurashima, M. Tateda, and Y. Koyamada, "Development of a distributed sensing technique using Brillouin scattering," J. Lightwave Technol. **13**, 1296–1302 (1995).
9. L. Thévenaz and S. F. Mafang, "Depletion in a distributed Brillouin fiber sensor: practical limitation and strategy to avoid it," Proc. SPIE **7753**, 77535A (2011).
10. W. Zou, Z. He, and K. Hotate, "Two-dimensional finite-element modal analysis of Brillouin gain spectra in optical fibers," IEEE Photon. Technol. Lett. **18**, 2487–2489 (2006).
11. L. Ursini, M. Santagiustina, and L. Palmieri, "Polarization-dependent Brillouin gain in randomly birefringence fibers," IEEE Photon. Technol. Lett. **22**, 712–714 (2010).
12. M. O. van Deventer and A. J. Boot, "Polarization properties of stimulated Brillouin scattering in single-mode fibers," J. Lightwave Technol. **12**, 585–590 (1994).
13. W. Zou, Z. He, and K. Hotate, "Complete discrimination of strain and temperature using Brillouin frequency shift and birefringence in a polarization-maintaining fiber," Opt. Express **17**, 1248–1255 (2009).
14. A. Zadok, A. Eyal, and M. Tur, "Polarization attributes of stimulated Brillouin scattering slow light in fiber," Proc. SPIE **7949**, 79490A (2011).
15. S. Xie, M. Pang, X. Bao, and L. Chen, "Polarization dependence of Brillouin linewidth and peak frequency due to fiber inhomogeneity in single mode fiber and its impact on distributed fiber Brillouin sensing," Opt. Express **20**, 6385–6399 (2012).
16. L. Thevenaz, M. Facchini, A. Fellay, M. Nikles, and P. Robert, "Evaluation of local birefringence along fibres using Brillouin analysis," in *Conference Digest OFMC'97* (National Physics Laboratory, 1997), pp. 82–85.
17. A. Zadok, S. Chin, L. Thevenaz, E. Zilka, A. Eyal, and M. Tur, "Polarization-induced distortion in stimulated Brillouin scattering slow-light systems," Opt. Lett. **34**, 2530–2532 (2009).
18. D. Williams, X. Bao, and L. Chen, "Characterization of high nonlinearity in Brillouin amplification in optical fibers with applications in fiber sensing and photonic logic," Photon. Res. **2**, 1–9 (2014).
19. L. Chen and X. Bao, "Analytical and numerical solutions for steady state stimulated Brillouin scattering in a single-mode fiber," Opt. Commun. **152**, 65–70 (1998).
20. E. Collette, *Field Guide to Polarization* (SPIE, 2005).
21. A. Kumar and A. Ghatak, *Polarization of Light with Applications in Optical Fibers* (SPIE, 2011).
22. Y. Li, X. Bao, Y. Dong, and L. Chen, "A novel distributed Brillouin sensor based on optical differential parametric amplification," J. Lightwave Technol. **28**, 2621–2626 (2010).
23. J. W. D. Chi, L. Chao, and M. K. Rao, "Time-domain large-signal investigation on nonlinear interactions between an optical pulse and semiconductor waveguides," IEEE J. Quantum Electron. **37**, 1329–1336 (2001).
24. R. Chu, M. Kanefsky, and J. Falk, "Numerical study of transient stimulated Brilllouin scattering," J. Appl. Phys. **71**, 4653–4658 (1992).
25. M. Razaghi, V. Ahmadi, and M. J. Connelly, "Comprehensive finite-difference time-dependent beam propagation model of counterpropagating picosecond pulses in a semiconductor optical amplifier," J. Lightwave Technol. **27**, 3162–3174 (2009).
26. F. S. Gokhan, G. W. Griffiths, and W. E. Schiesser, "Method of lines solution to the transient SBS equations for nanosecond Stokes pulses," J. Eur. Opt. Soc. **8**, 13049 (2013).
27. Z. Zhu, D. J. Gauthier, Y. Okawachi, J. E. Sharping, A. L. Gaeta, R. W. Boyd, and A. E. Willner, "Numerical study of all-optical slow-light delays via stimulated Brillouin scattering in an optical fiber," J. Opt. Soc. Am. B **22**, 2378–2384 (2005).
28. C. Zeringue, I. Dajani, S. Naderi, G. T. Moore, and C. Robin, "A theoretical study of transient stimulated Brillouin scattering in optical fibers seeded with phase-modulated light," Opt. Express **20**, 21196–21213 (2012).
29. D. Cotter, "Transient stimulated Brillouin scattering in long single-mode fibres," Electron. Lett. **18**, 504–506 (1982).
30. V. P. Kalosha, L. Chen, and X. Bao, "Slow and fast light via SBS in optical fibers for short pulses and broadband pump," Opt. Express **14**, 12693–12703 (2006).
31. V. P. Kalosha, E. A. Ponomarev, L. Chen, and X. Bao, "How to obtain high spectral resolution of SBS-based distributed sensing by using nanosecond pulses," Opt. Express **14**, 2071–2077 (2006).

32. S. V. Afshar, G. A. Ferrier, X. Bao, and L. Chen, "Effect of the finite extinction ratio of an electro-optic modulator on the performance of distributed probe-pump Brillouin sensor systems," Opt. Lett. **28**, 1418–1420 (2003).
33. R. Bernini, A. Minardo, and L. Zeni, "Dynamic strain measurement in optical fibers by stimulated Brillouin scattering," Opt. Lett. **34**, 2613–2615 (2009).
34. X. Bao, C. Zhang, W. Li, M. Eisa, S. El-Gamal, and B. Benmokrane, "Monitoring the distributed impact wave on a concrete slab due to the traffic based on polarization dependence on stimulated Brillouin scattering," Smart Mater. Struct. **17**, 015003 (2008).
35. V. I. Kovalev and R. G. Harrison, "Observation of inhomogeneous spectral broadening of stimulated Brillouin scattering in an optical fiber," Phys. Rev. Lett. **85**, 1879–1882 (2000).
36. L. Stepien, S. Randoux, and J. Zemmouri, "Origin of spectral hole burning in Brillouin fiber amplifiers and generators," Phys. Rev. A **65**, 053812 (2002).